PCCP

PAPER

View Article Online
View Journal

Cite this: DOI: 10.1039/c4cp00075g

Local bias induced ferroelectricity in manganites with competing charge and orbital order states†

Fábio G. N. Figueiras,*[a] Igor K. Bdikin,[b] Vitor B. S. Amaral[a] and Andrei L. Kholkin[c]

Received 7th January 2014,
Accepted 15th January 2014

DOI: 10.1039/c4cp00075g

www.rsc.org/pccp

Perovskite-type manganites, such as $Pr_{1-x}Ca_xMnO_3$, $La_{1-x}Ca_xMnO_3$ and $La_{1-x}Sr_xMnO_3$ solid solutions, are set forth as a case study of ferroelectricity formation mechanisms associated with the appearance of site- and bond-centered orbital ordering which breaks structural inversion symmetry. Even though the observation of macroscopic ferroelectricity may be hindered by the finite conductivity of manganites, polarization can still exist in nanoscale volumes. We use Piezoresponse Force Microscopy to probe local bias induced modifications of electrical and electromechanical properties at the manganite surface. Clear bias-induced piezocontrast and local hysteresis loops are observed for $La_{0.89}Sr_{0.11}MnO_3$ and $Pr_{0.60}Ca_{0.40}MnO_3$ compounds providing convincing evidence of the existence of locally induced polar states well above the transition temperature of the CO phase, while the reference samples without CO behavior show no ferroelectric-like response. Such coexistence of ferroelectricity and magnetism in manganites due to the charge ordering (CO) under locally applied electric field opens up a new pathway to expand the phase diagrams of such systems and to achieve spatially localized multiferroic effects with a potential to be used in a new generation of memory cells and data processing circuits.

Introduction

Manganites present a wide spectrum of structural and functional phases[1,2] associated with the competing charge, lattice, orbital and spin degrees of freedom, and become an excellent test ground for modification of materials. Multifunctional behavior can be achieved through careful chemical manipulation, resulting in colossal magnetoresistance (CMR), ferroelectricity (FE), conductivity behavior, complex magnetic states and structural symmetries,[3,4] whereas various phase transitions can be induced by means of external factors (temperature, pressure, and magnetic and electric fields).[5,6] In the case of manganites possessing simultaneously charge and orbital order (CO/OO) properties, the occurrence of particular electronic spatial modulations (bond or spin dimerization), which present simultaneous site inequivalency and bond distortion, may allow breaking structural inversion symmetry potentially leading to ferroelectricity.[7,8] However, manganites generally present relatively low specific resistivity making conventional dielectric measurements not viable due to extensive conductivity loss. Such CO/OO states that are estimated to co-exist should in general have energy levels very close to one another and were only found to be active at low temperatures in the conventional phase diagram; nonetheless, localized FE effects (10 nm scale) can be studied *via* Piezoresponse Force Microscopy (PFM) and particularly, bias lithography techniques can be used to induce phase transition in selected regions of the material surface.[9] In its turn, Band Excitation Piezoresponse Spectroscopy (BEPS) is a useful tool to testify and quantify the presence of locally induced ferroelectricity and verify the possibility of charge accumulation or electrochemical phenomena;[10,11] in addition, current *vs.* voltage (*I–V*) probing enables us to inspect injection/mobility of charge carriers in the subsurface region.

The phase diagrams of $Pr_{1-x}Ca_xMnO_3$,[4] $La_{1-x}Sr_xMnO_3$[11,12] and $La_{1-x}Ca_xMnO_3$[3] manganites present for each system some particular doping composition regions (in x) having rich transition thresholds between insulating and/or CO/OO property states also correlated with Insulator–Metal transition and even magnetic ordered phases; these transitions are easily affected by external perturbations, and could reveal complex dielectric/magnetic/structural response behaviors. Inspiring research studies can be found in the work of Jooss,[13] which identifies localized bias induced structural transitions and introduces a further insight into the $Pr_{1-x}Ca_xMnO_3$ system, extending to $0.3 < x < 0.5$, having simultaneous charge and antiferromagnetic orders below T_N, imposing cooperative Jahn–Teller (JT) distortions leading to a non-centrosymmetric $P2_1nm$ structure, hence meeting some of the requisites to be classified as intrinsic type I

[a] Physics Department & CICECO, University of Aveiro, 3810-193 Aveiro, Portugal. E-mail: ffigueiras@ua.pt; Fax: +351 234 401 470; Tel: +351 234 372 571
[b] Mechanics Eng. Department & TEMA, University of Aveiro, 3810-193 Aveiro, Portugal. Fax: +351 234 370 953; Tel: +351 234 370 830
[c] Materials Eng. Ceramics Department & CICECO, University of Aveiro, 3810-193 Aveiro, Portugal

† Electronic supplementary information (ESI) available: Gray scale contrast version of coloured Fig. 3 and 4 found online. See DOI: 10.1039/c4cp00075g

multiferroic and making it one of the best candidates to prove a promising model of induced FE effects in manganites. In addition, electric field gradient (EFG) studies of A. Lopes *et al.*[14] across the $Pr_{1-x}Ca_xMnO_3$ phase diagram, using hyperfine Perturbed Angular Correlation (PAC) measurements with ^{111m}Cd, revealed typical signatures of a phase transition involving long-range ordering of local dipoles over the entire CO/OO region. Previous bias lithography and PFM experiments performed in a single crystal $La_{0.89}Sr_{0.11}MnO_3$ sample also provide a reference for this study.[15] The FE localized phenomenon shows important scientific promise for creating artificial multiferroic materials and memory states.

Experimental

A selection of manganite samples having compositions near CO/OO transition thresholds and also some without CO/OO (control) samples[11,16] include single crystals prepared by a floating zone method and polycrystals prepared by a solid state process comprising $La_{1-x}Sr_xMnO_3$ (x = 0.11, 0.30), $Pr_{1-x}Ca_xMnO_3$ (x = 0.00, 0.35, 0.40, 0.85) and $La_{1-x}Ca_xMnO_3$ (x = 0.05; 0.33). Experiments were performed using several PFM systems including *Asylum*®, *PicoPlusTM*®, *Agilent*®, *NT-MDT*® and *Veeco*®. The general procedure consists of selecting a 5 × 5 μm region with regular topology, then sketching a lithographic frame of 2 μm length separated lines traced at ~100 nm s^{-1} at different bias voltages (up to ±30 $V_{d.c.}$), as schematized in Fig. 1. The tip pressure is adjusted to avoid scratching of the surface while maximizing electrical contact. Further BEPS mapping, piezocontrast imaging, localized piezoresponse loops, and *I–V* curve measurements between ±10 $V_{d.c.}$ (up to 20 nA detection maximum) enable us to trace particular effects to stimulated regions.

Fig. 1 Schematic of bias lithographic paths in a 5 × 5 μm^2 of sample surface.

Results and discussion

Extensive lithographic experiments and PFM measurements were carried out in several samples. In general, subsequent to the bias lithographic tests, topological mapping shows no relevant mechanical deformation of the surface, enabling us to discriminate the piezoresponse contrast that appears in the respective lithographed paths from topological cross-talk effects. Graphs of Fig. 2a and b enable us to abridge typical piezoresponse loops averaged from the regions subjected to local poling in comparison to the non-stimulated areas. BEPS measurements gather a widespread sequence of amplitude and phase data obtained for each pixel as a function of the probing frequency and bias voltage; this method enables data acquisition having unambiguous decoupling of the conservative and dissipative interactions, removing topographic cross-talk and allowing identification of non-linear responses. The contours and contrasts found in the set of parameter maps depicted in the BEPS measurements of Fig. 3 and 4 can be interpreted as changes in behavior of the loop profiles within the bias lithographed regions compared to the non-stimulated surface, inferred from charting nucleation sites, energy dissipation on polarization switching, saturation (R±) and coercive (V±) FE parameters.[10]

Fig. 3 shows PFM and BEPS scans performed for a $Pr_{0.60}Ca_{0.40}MnO_3$ sample measured at room temperature in the paramagnetic phase and above the CO/OO transition.

Experimental lithographic bias lines poling at +10 and −10 V gave rise to opposite piezoelectric contrast, evidencing the formation of a local polar state, without visible effects on the surface topography of the sample. The polarization relaxes after a few hours, a time scale much longer than that expected for transient trapped charges.

The experiments performed in the $La_{0.89}Sr_{0.11}MnO_3$ monocrystalline sample and the PFM scans in Fig. 4 testify how local piezoresponse signals are directly traceable to the lithographic path stimulated regions. It is possible to observe that the lithographic paths made under negative bias voltage induce

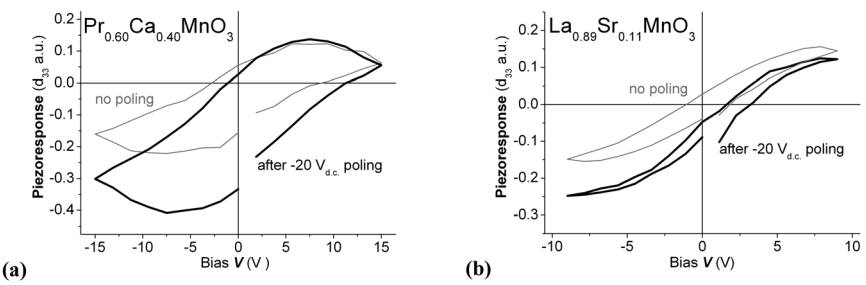

Fig. 2 Comparison between typical piezoresponse loops from the distinct regions of the (a) $Pr_{0.60}Ca_{0.40}MnO_3$ and (b) $La_{0.89}Sr_{0.11}MnO_3$ samples, before and after poling bias lithography.

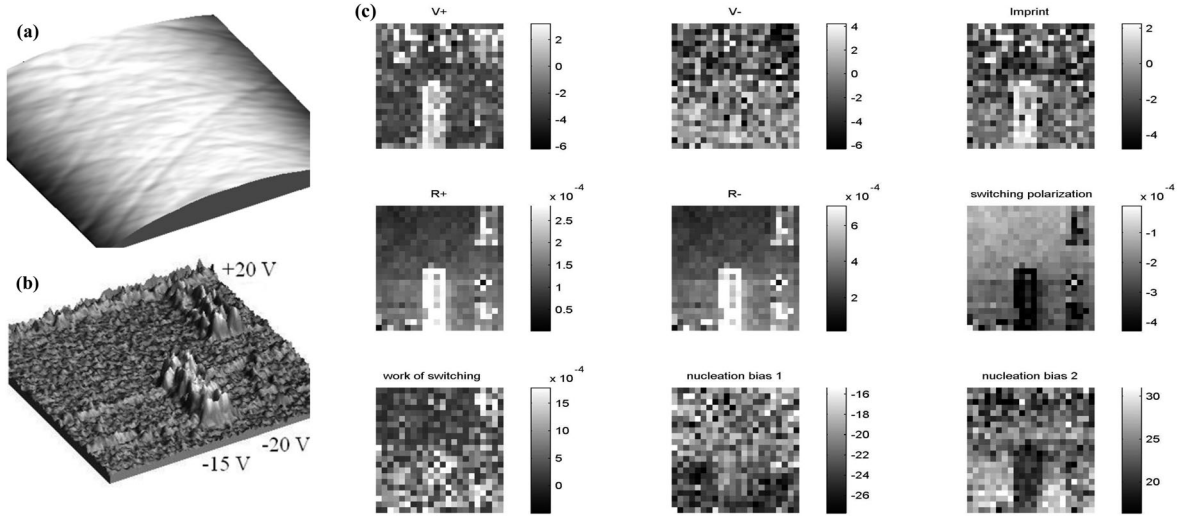

Fig. 3 Topographic (a) and piezocontrast (b) scans of a 3 × 3 μm^2 surface after performing bias lithographic paths; details of the respective BEPS map results (c) for the single crystal $Pr_{0.60}Ca_{0.40}MnO_3$ sample.

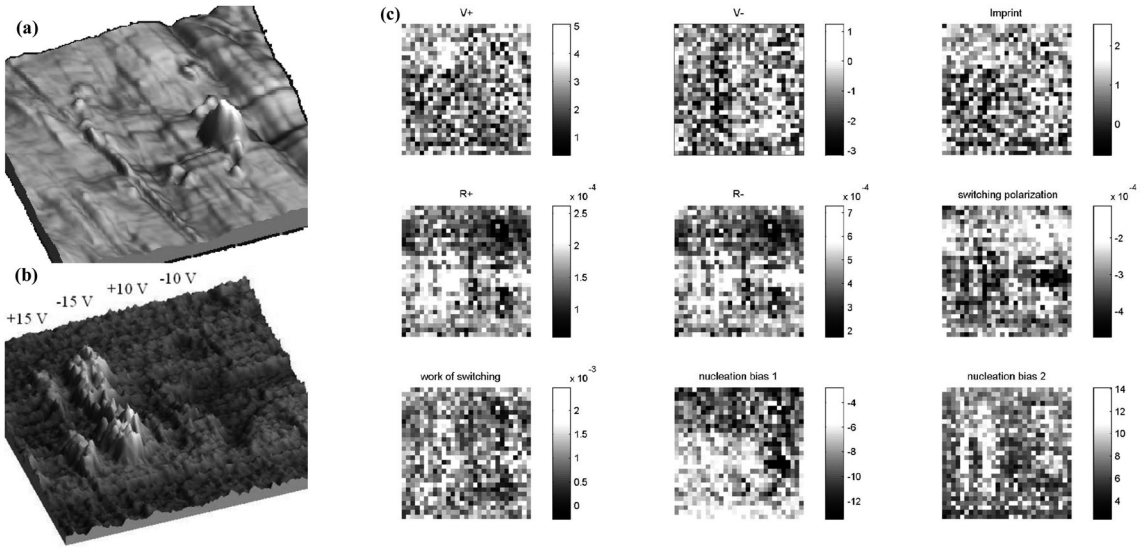

Fig. 4 Topographic (a) and piezocontrast (b) scans of a 3 × 3 μm^2 surface after performing bias lithographic paths; details of the respective BEPS map results (c) for the single crystal $La_{0.89}Sr_{0.11}MnO_3$ sample.

stronger piezoresponse contrast on the sample surface than the positive bias; such asymmetric response of the sample is coherent with the *I–V* experiments further discussed. No reaction was detected from the +10 $V_{d.c.}$ litho path; a minor surface alteration can be detected at the end of the path made at −10 $V_{d.c.}$ due to incidental parking of the tip and should not be considered relevant, since the bulging is not extended to the rest of the stimulated region.

For the other manganite samples having compositions that also allow CO/OO states, namely, the nominal $Pr_{0.65}Ca_{0.35}MnO_3$, $Pr_{0.15}Ca_{0.85}MnO_3$ and $La_{0.05}Ca_{0.95}MnO_3$, respective PFM measurements reveal some circumspect piezoresponse contrast traceable mainly to the negative lithographic paths, not enough to be considered as substantial BEPS results to be reported, nevertheless, some details are noteworthy. The monocrystalline $Pr_{0.65}Ca_{0.35}MnO_3$ sample does not react at lithographic bias fields smaller than |±20| $V_{d.c.}$; some scarce surface bulging from the tip passage at −20 $V_{d.c.}$ could be observed, nevertheless the piezoresponse amplitude contrast is homogeneous all along the path, enabling again to discard cross-talk interference, hence attesting the correlation to a change in the dielectric properties and not due to mechanical/chemical features; for the +20 $V_{d.c.}$ litho path the piezoresponse amplitude changes signal, pointing again to poling effects on the material. For these two samples the respective CO/OO states lie at a lower temperature (T_{CO} ∼210 K for x = 0.35 and T_N = 120 K for x = 0.85), both are chemically much closer to the paraelectric composition threshold (x = 0.3 and x = 0.9 respectively), hence metastable ordered states become easily dispersed under room temperature thermodynamic conditions.

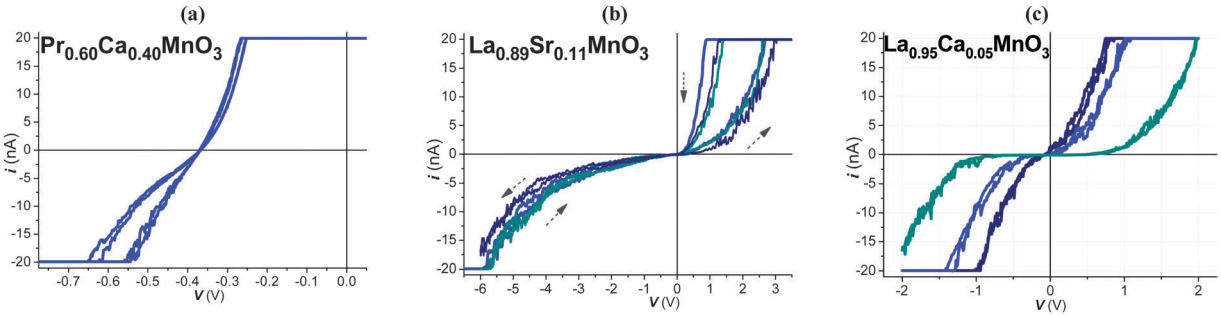

Fig. 5 Representative *I–V* curve measurements at distinct surface points of the $Pr_{0.60}Ca_{0.40}MnO_3$ (a), $La_{0.89}Sr_{0.11}MnO_3$ (b), and $La_{0.95}Ca_{0.05}MnO_3$ (c) samples.

For the $La_{0.95}Ca_{0.05}MnO_3$ sample the piezocontrast observed over the stimulated regions is essentially due to a signal phase shift without significant amplitude increase in comparison to the non-stimulated regions. These alterations of dielectric properties are only partially revealed in BEPS maps, but not attaining such clear switching and saturation parameters such as those described for the $Pr_{0.60}Ca_{0.40}MnO_3$ and $La_{0.89}Sr_{0.11}MnO_3$ samples.

The symmetric behavior of the *I–V* curves shown in Fig. 5(c) suggests more conventional low conductivity phenomena.

The most pertinent fact is that equivalent bias lithographic tests (up to ± 30 $V_{d.c.}$) performed in conventional dielectric oxides like Mn_3O_4 or $PrMnO_3$, $La_{0.67}Ca_{0.33}MnO_3$ and $La_{0.7}Sr_{0.3}MnO_3$ manganites did not lead to any piezoresponse signal or BEPS contrast maps. These complementary observations in the reference compounds suggest that possible capacitive effects or electrochemical surface reaction promoted by the highly localized and intense electric field[11,17] might not be the only phenomena accountable for the responses described for samples $Pr_{0.60}Ca_{0.40}MnO_3$ and $La_{0.89}Sr_{0.11}MnO_3$.

The reckonable local alterations of the dielectric properties of these CO/OO series of manganite samples under the lithographic bias stimulation neither follow conventional Ohm's law[18] nor Frenkel's law[19] where an increase in conductivity could be expected upon lowering the activation energy of the carrier when applying an electric field. In fact, higher electric conductivity manganite control samples such as $La_{0.67}Ca_{0.33}MnO_3$ renders any charge accumulation induced by the PFM tip to be rapidly dispersed in the material and dissipated through the sample holder electrode.

Some additional insight into the local effect of the bias poling on the surface state of the sample can be perceived from *I–V* probing measurements.[20] The relatively high resistivity found at the surface of the CO/OO type manganite series of samples ($>10^3$ Ω mm) restricted the experimental conditions within distances of a few μm between the tip and the sample holder electrode across the sample surface. Measurements are performed at 0.1 Hz ramps between ±10 V in order to establish a quantifiable current ($0.1\ \text{nA} < i < 20\ \text{nA}$), as well as to distinguish and to prevent inconsistent pA charge–discharge loops arising from an undesirable equivalent capacitor circuit from the system set-up.

The *I–V* measurements were repeated at several points of the samples surface, of which most consistent and representative results are shown in the graphs in Fig. 5. The reproducibility and the number of cycles through the curves have certain limitations due to progressive tip wearing and degradation of the sample surface as expected due to mechanical stress and current leakage/heating in addition to other hampering factors like surface inhomogeneities and hydration adsorbed layers.

An important trend that can be observed for the $Pr_{0.60}Ca_{0.40}MnO_3$ and $La_{0.89}Sr_{0.11}MnO_3$ samples is the asymmetric shape and hysteresis of the current response to the applied bias voltage in contrast to the symmetric behavior described for normal metal–manganite heterojunctions.[20] These asymmetries are revealed in the delay of current response to low negative bias voltage which can be related to the different availability and mobility of the charge carriers, electrons (polarons) or holes in the material, reminding of a semiconductor p–n junction and a Zener like effect. In its turn, the current inversion hysteresis can be associated with the inversion of the FE domains; in fact, the initial set of bias probe voltages has a resolute influence on the outcome of the *I–V* measurements. When starting from −10 V the point effect on the sample surface can induce a localized FE state transition which leads to a dielectric behavior (no current flow) setting through the ramp up to +10 V, whereas starting from +10 V enables current flow and we observe a finite number of t *I–V* curves as testified in the respective left and center graphs in Fig. 5.

These expressive PFM sets of results are an indication that in addition to local electrochemical oxygen diffusion phenomena, additional mechanisms can also be evolved, in particular for manganite systems possessing CO/OO states. The highly confined electric field and a partial injection and trapping of charge carriers can reorganize the local polaronic distribution (modulated strain/electron/spin),[21] usually found in thermodynamic disarray at room temperature, hence promoting the expansion of a particular metastable state which can be detected by a dielectric/ferroelectric signature in contrast to the electrical properties of the conventional host phase.[22–24] The formation of these embedded charge/orbital and antiferromagnetic orders prevent electron hopping, and the correlations can survive locally as "Zener polarons"[25,26] above T_{CO} and

even T_N. Under these circumstances Mn ions and Mn–O–Mn bonds become nonequivalent resulting in a noncentrosymmetric electronic structure which is prone to exhibit some piezoelectric response.

Conclusions

The present PFM studies performed at room temperature demonstrated that by means of suitable bias lithography stimulation, it is possible to induce and stabilize localized states which exhibit a clear piezocontrast, possibly associated with the presence of nanoscopic CO/OO regions beyond the thermodynamic conditions of the conventional phase diagram. SPM methods can be extended to variables such as magnetic and electric properties and temperature and time responses; combined with other local probe techniques like hyperfine spectroscopies and theoretical modeling, it can bring new insights into correlated electron systems, opening new pathways to study local scale multiferroic phenomena originating from complex charge/orbital ordering effects in materials particularly susceptible to phase transitions under localized disturbance. Understanding the mechanisms that underlie such complex processes along with optimizing the technical procedures and design of materials in order to reach room temperature stabilization of the modifications ultimately lead to the design of artificial multiferroic materials and memory cells.

Acknowledgements

This work was supported by FCT and COMPETE/FEDER through projects PTDC/FIS/105416/2008 MULTIFOX and PEst-C/CTM/LA0011/2013, and Grants SFRH/BD/25011/2005 and SFRH/BPD/80663/2011. The authors thank S. Kalinin, P. Maksymovych, S. Guo, K. Seal, S. Jesse, N. Balke and M. Nikiforov for ONRL CNMS proposal CNMS2009-083. The authors also acknowledge Y. Tokura for the supply of the single crystal Pr–Ca manganite samples and P. B. Tavares for the La–Ca manganites.

Notes and references

1 J. M. D. Coey, M. Viret and S. von Molnar, *Adv. Phys.*, 1999, **48**(2), 167.
2 J. B. Goodenough, *Handbook on the Physics and Chemistry of Rare Earths*, 2003, ch. 214, vol. 33, pp. 249–351.
3 C. Martin, A. Maignan, M. Hervieu and B. Raveau, *Phys. Rev. B: Condens. Matter Mater. Phys.*, 1999, **60**, 17.
4 Y. Tokura, *Rep. Prog. Phys.*, 2006, **69**, 797.
5 E. Dagotto, T. Hotta and A. Moreo, *Phys. Rep.*, 2001, **344**, 1–153.
6 Y. Tomioka, A. Asamitsu, H. Kuwahara, Y. Moritomo and Y. Tokura, *Phys. Rev. B: Condens. Matter Mater. Phys.*, 1996, **53**, R1689–R1692.
7 J. Van Den Brink and D. I. Khomskii, *J. Phys.: Condens. Matter*, 2008, **20**, 434217.
8 D. V Efremov, J. Van Den Brink and D. I. Khomskii, *Nat. Mater.*, 2004, **3**, 853–856.
9 S. V. Kalilin, *et al.*, *Mater. Today*, 2008, **11**(11), 16–27.
10 S. Jesse, H. N. Lee and S. V. Kalinin, *Rev. Sci. Instrum.*, 2006, **77**(073702), 77–86.
11 S. V. Kalinin, A. Borisevich and D. Fong, *ACS Nano*, 2012, **6**(12), 10423–10437.
12 A. Urushibara, Y. Moritomo, A. Asamitsu, G. Kido and Y. Tokura, *Phys. Rev. B: Condens. Matter Mater. Phys.*, 1995, **51**, 14103.
13 C. Jooss, *et al.*, *Proc. Natl. Acad. Sci. U. S. A.*, 2007, **104**(34), 13597–13602.
14 A. M. L. Lopes, J. P. Araújo, V. S. Amaral, J. G. Correia, Y. Tomioka and Y. Tokura, *Phys. Rev. Lett.*, 2008, **100**, 155702.
15 R. F. Mamin, I. K. Bdikin and A. L. Kholkin, *Appl. Phys. Lett.*, 2009, **94**, 222901.
16 A. Asamitsu, Y. Tomioka, H. Kuwahara and Y. Tokura, *Nature*, 1997, **388**, 50–52.
17 M. Cherry, M. S. Islam and C. R. A. Catlow, *J. Solid State Chem.*, 1995, **118**, 125–132.
18 N. I. Solin, A. A. Samokhvalov and S. V. Naumov, *Phys. Solid State*, 1998, **40**(10), 1706–1709.
19 Ya. I. Frenkel, *Zh. Éksp Teor. Fiz.*, 1971, **8**, 1292.
20 N. A. Tulina, S. A. Zverkov, A. Arsenov, Y. M. Mukovskii and D. A. Shulyatev, *Physica C*, 2003, **385**, 563–567.
21 K. H. Ahn, T. Lookman and A. R. Bishop, *Nature*, 2004, **428**, 401–404.
22 A. Sergienko, C. Sen and E. Dagotto, *Phys. Rev. Lett.*, 2006, **97**, 227204.
23 N. Panwar, I. K. Bdikin, A. N. Morozovska and A. L. Kholkin, *J. Appl. Phys.*, 2012, **112**, 052019.
24 N. Panwar, I. Coondoo and A. L. Kholkin, *Solid State Commun.*, 2013, **164**, 38–41.
25 L. Wu, R. F. Klie, Y. Zhu and C. Jooss, *Phys. Rev. B: Condens. Matter Mater. Phys.*, 2007, **76**, 174210.
26 T. Mizokawa, *Nanoscale Res. Lett.*, 2012, **7**, 582.